Gamma Ray Index – Shale Volume Transforms

David Kennedy, *QED* Petrophysics LLC

ABSTRACT

Although a relationship between gamma ray log response and shale volume had been recognized since the introduction of gamma ray logging in the late 1930s and early 1940s, the formula for gamma ray index, and the equating of gamma ray index to shale volume apparently appeared in the late 1960s. Contemporaneously there appeared three similar, alternative, non-linear relationships in 1969, 1970, and 1971. These functions were based upon observations and empirical graphical functions. Subsequently, these graphical functions were fit using very dissimilar-looking formulas. Only the 1969 data set was published in support of the graphical functions. No attempt to link these functions with a single formula was ever made, and only vague verbal explanations have been offered for the non-linear functions. Further, the 1969 publication was in Russian, partly mistranslated, and the mistranslation never corrected. Consequently, two of the resulting formulas are misapplied.

In this article I review the four standard non-linear functions (i.e., Larionov's two, Stieber's, Clavier's), examine their similarities, and show that a single function would serve the same purpose as all four, thereby eliminating a source of confusion for formation evaluators.

When these shale (or clay) volume versus gamma ray index transforms are inverted to functions of gamma ray index versus shale (or clay) fractional volume a remarkable property is revealed: the increment of radioactivity per unit shale volume decreases with increases in fractional shale volume. In other words, if one unit of shale per unit volume produces a gamma ray intensity of 10 API units we would think it strange if 10 units of shale per unit volume produced only, say, 60 API units of gamma radiation (instead of 100). Yet, this is the message contained in these functions. The cause for this phenomenon has been speculated upon, but only briefly and not often.

To remedy this lack of speculation, I propose a physical model and give it mathematical form. This model is intended as a challenge to theoretical-minded petrophysicists to falsify it, make it better, or propose an alternative and more realistic model. I also provide (in Appendix C) a digital listing of all the published graphical data in the literature that support the introduction of the non-linear shale (and clay) fractional volume – gamma ray index transforms.

INTRODUCTION

Radioactivity in rocks originates mainly with the radionuclides thorium 232, uranium 238, potassium 40, and the daughter nuclei in their respective radioactive decay sequences. Uranium 235 is also a minor contributor. The primary disintegration for thorium and uranium is by means of emission of alpha particles (i.e., helium nuclei), followed in their decay sequences by further emissions of alpha particles, beta particles (electrons and positrons), and high-frequency electromagnetic photons called gamma rays. Together, these emissions are called "radioactivity". In the case of potassium, a proton in the nucleus captures an electron, transmuting the nucleus to argon and emitting a gamma ray photon.

It is not generally known that radioactive element abundance is relatively high. For example, potassium is the 7th most abundant element in the earth's crust, about 1 percent of which is potassium 40. The isotope is relatively stable, with a half-life of 1.2 billion years. Potassium is an element necessary for life and this means that organisms contain a fraction of radioactive potassium. For each 100 pounds of body mass there are 2800 potassium disintegrations per second, each second, for life, and after life ends for that matter.

Estimates of concentration of uranium vary with 5 ppm being an average computed from several internet sources. Sources agree that thorium is about three times as abundant as uranium. For comparison to more familiar elements, uranium is 30 times more common than silver and 600 times more common than gold. By comparison with gold, uranium and thorium are not rare.

Of interest for this study is the occurrence of radioactive elements in certain types of sedimentary rocks. Feldspars (orthoclase, microcline, sanidine) containing potassium originate in igneous rocks. The decomposition of these rocks due to weathering can lead to the inclusion of feldspars in arkosic sandstones. However, the most common

occurrence in sedimentary rocks is the association of clay minerals and radioactive elements and minerals. Clay crystals are negatively charged macro-anions which attract positively charged cations with the potassium ion fitting nicely into dimples on some clay crystal surfaces. In addition, uranium precipitates from sea water under the same conditions that favor deposition of organic materials and is thus enriched in shales, particularly organic shales. Abundant thorium is associated with resistate minerals included in shales but details of its occurrence are not found in the oilfield literature. The description in the SEG-Wiki is typical: "Thorium, . . . is insoluble and occurs in almost constant values in shales because of this property. A typical shale will have a thorium range from 8-18 ppm, with thorium contributing anywhere from 40-50% of the radioactivity." Followed by the summarizing assertion: "a shale is typically associated with a high radioactivity made up primarily by thorium, to a lesser extent potassium, and a variable amount of uranium." As you see, the description offers no details regarding how the thorium is deposited in the shale or where it resides thereinafter; this lack of detail is typical.

Gamma ray logging began in the late 1930s and early 1940s. Gamma ray intensity for use in estimating shale volumes is documented in the literature perhaps beginning in 1951 (Bush and Mardock). Surprisingly, a succinct formula for the gamma ray index in its modern format does not appear until nearly two additional decades had passed. The earliest occurrence of

$$I_{GR} = \frac{GR_{log} - GR_{min}}{GR_{max} - GR_{min}} = V_{clay} \qquad (1)$$

may have been in the paper by Poupon and Gaymard (1970). Heslop (1974) refers to "the classical method of calculating shale volume from the gamma-ray log," and is probably referring to equation (1) as the "classical" method (the name suggestive of a significant history for the method), but does not give a formula for the method in his paper. If indeed he refers to (1), it seems improbable that it could have become a "classic" in a mere four years, suggesting it had been in use for a long time, regardless that it appears to have not been published till 1970.

Poupon and Gaymard do not refer to a "gamma ray index" but present the ratio of differences directly as fractional shale volume. If one assumes that gamma ray intensity is proportional to the amount of clay and that all clay is equally radioactive, it follows that the gamma ray index should scale directly with clay volume. And, indeed, it is used in this way as one of the clay (or shale) indicators.

Clay volume and shale volume have often been used as if they are synonymous, but they are not. Shale is a mixture of silt sized grains of rock-forming minerals (such as quartz) and clay crystals. They are deposited together due to size similarity. The fractional volumes of the silt and clay fractions vary from shale-to-shale. Further, the silt component can also contribute to the radioactivity, depending upon its mineralogical composition. For one example, silt sized zircon can be many times more radioactive than an equal volume of clay. A relatively minor fraction of radioactive silt could spoil the linear relationship between gamma ray index and clay volume. Further, while the maximum and minimum amounts of clay and shale may coincide, the fractional clay volume will be less than the fractional shale volume unless the formation is 100 percent clay. Typical clay volumes are about 60 percent of shale volume (Bhuyan and Passey, 1994).

Contemporaneous with the above efforts, pulsed neutron log interpreters were discovering that the assumption of a linear relationship between gamma ray intensity of clay volume (Larionov, 1969) or shale volume (Stieber, 1970; Clavier et al., 1971) was inconsistent with their results. These authors published similar-looking non-linear graphical functions for relating clay and shale volumes (respectively) to gamma ray intensity.

Stieber provided a formula for his suggested transform, although Stieber's transform is in terms of the complement of the gamma ray index; i.e., $1 - I_{GR}$. Formulas for Larionov's and Clavier's graphical transforms were later introduced anonymously (e.g., in service company literature).

TRANSFORMS

Larionov. V. V. Larionov's 1969 book, *Borehole Radiometry* (in Russian), was first to publish evidence for a non-linear relationship between gamma ray index and clay volume. Of the three seminal references on this topic, Larionov's is the only one to publish data. Two data sets are included in his discussion of clastic rocks (he also included a discussion of carbonates, omitted herein). These data are grouped by region and age, as explained in the captions to Larionov's figures 23 and 43. I provide my translations to these captions in figures 1 and 2. (See also Appendix D.) Larionov's digitized data is shown in figures 3 and 4.

As you see, there are two data sets, and two interpretation charts. These have been distinguished in the western

literature for a half century as being for Tertiary and "older" rocks. I have emphasized the time terms in the translations with boldface type. As you see, the actual distinction in the original is between Paleozoic and Mesozoic/Tertiary. In fact, Mesozoic is specified in the captions of both figures 23 and 43, whereas Tertiary is mentioned only in the caption to figure 43.

Larionov does not fit his data with equations, but as his work became a part of the list of gamma ray index – shale volume transforms a formula was invented. I have been unable to identify the first publication. For Mesozoic and Cenozoic (tertiary) rocks Larionov's data is fit using

$$V_{clay} = 0.083\left(2^{(3.7 I_{GR}-1)}\right). \qquad (2)$$

For his Paleozoic data, the fit is modeled by

$$V_{clay} = 0.33\left(2^{(2 I_{GR}-1)}\right). \qquad (3)$$

Stieber. The Stieber paper from 1970, *Pulsed Neutron Capture Log Evaluation: Louisiana Gulf Coast,* employed data from the U. S. Gulf (of Mexico) coast region. Stieber found the linear relationship did not produce interpretable results.

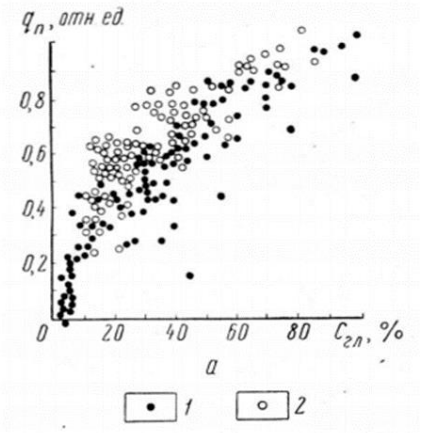

Рис. 23. Связь естественной радиоактивности q_n терригенных отложений с глинистостью $C_{гл}$
1 — палеозойские отложения Предуралья и центральных районов СССР; *2* — мезозойские отложения южных районов СССР

Fig. 23. Relationship (of) natural radioactivity q_n (to) terrigenous sediment with clay $C_{гл}$.
1 – **Paleozoic** sediments from Pre-Urals and central areas of the USSR. 2 – **Mesozoic** sediments from the southern USSR.

Figure 1. The first, and so far only (and therefore seminal), data sets suggesting non-linear gamma ray index – shale volume transforms.

Stieber formulated his correction in terms of a "sand fraction" $F(\gamma)$, where γ is a "sand index" $\gamma = 1 - I_{GR}$. The resulting formula is

$$V_{sh} = \frac{I_{GR}}{3 - 2I_{GR}}. \qquad (4)$$

Stieber does not provide his data (figure 5), but he informs his readers "This relationship was developed by trial and error …".

Clavier et al. Lastly, in 1971, Clavier and coauthors working with Middle Eastern sandstones and pulsed neutron data, in their paper "*Quantitative Interpretation of Thermal Neutron Decay Time Logs*: *Part I. Fundamentals and Techniques*" found similarly to Stieber that a non-liner gamma ray index – shale volume transform was necessary. This transform is published only as a graphical function with the justification "… use of the empirical chart … [figure 6] was found more reliable than assuming linearity between gamma ray log and shale volume." No equation was published with the graphical function.

The Clavier et al. curve has been fit (anonymously) using

$$V_{sh} = 1.7 - \sqrt{3.38 - \left(I_{GR} + 0.7\right)^2}. \qquad (5)$$

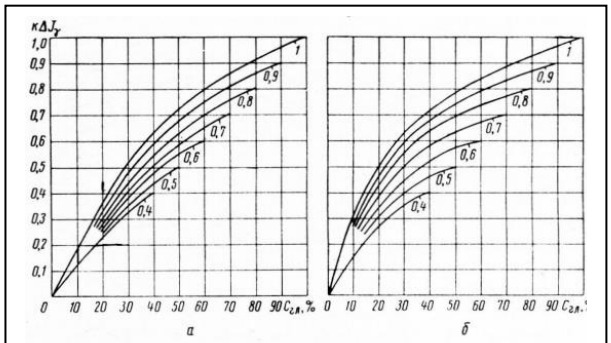

Рис. 43. Палетки для приближенной оценки глинистости осадочных горных пород.
а — для палеозойских отложений Предуралья и центральных районов Европейской части СССР; *б* — для мезозойских и третичных отложений южных районов СССР. Шифр кривых — поправочный коэффициент k.

Fig. 43. Charts for the evaluation of argillaceous sedimentary rocks.
a – For **Paleozoic** sediments from the Pre-Urals and central European regions of the USSR; *b* – For **Mesozoic** and **Tertiary** sediments from the southern region of the USSR.

Figure 2. The first interpretation of the non-linear relationship between gamma ray intensity and clay volume.

Summary of Transforms. The legacy that these authors have bequeathed to us is one data set, four curves, and four equations. In spite of the similarity of the curves, the fitting functions are quite different. Since they are fitting functions, there is no physics to be found in these functions; thus, they are mathematically quite dissimilar forms. Nor is Stieber's and Clavier's data available for comparison and analysis. Nevertheless, this leads to the question of whether the four functions could be replaced by a single fitting function.

The formulas can be generalized as a family of one-parameter fitting functions. The generalized form of Larionov's formula is

$$V_{clay} = \frac{2^{AI_{GR}} - 1}{2^{A} - 1}. \qquad (6)$$

where A = 2 for Paleozoic rocks in the European USSR, and A = 3.7 for the Mesozoic and Cenozoic of the southern USSR.

The generalization of the Stieber and Clavier formulas are

$$V_{sh} = \frac{I_{GR}}{B - (B-1)I_{GR}}. \qquad (7)$$

and

$$V_{sh} = (C+1) - \sqrt{\left[(C+1)^2 + C^2\right] - (I_{GR} + C)^2} \qquad (8)$$

respectively. By varying A, B, and C one is able to compare the locus of the curves so generated and note the functions really do produce very similar curves.

The Larionov formula uses A = 3.7 for Mesozoic and Cenozoic rocks, and A = 2 for Paleozoic rocks. A = 2.4 closely mimics the Clavier curve; A = 3.3 closely mimics the Stieber curve. Of course, varying 2 < A < 3.7 produces a plethora of possible fitting curves between the limits set by the Larionov function.

Similarly, B = 2, B = 2.3 and B = 3.4 reproduces Larionov Paleozoic, Clavier et al., and Larionov Mesozoic and Cenozoic curves, and C = 0.95, C = 0.38, and C = 0.30, reproduces Larionov Paleo, Stieber, and Larionov Meso and Cenozoic curves.

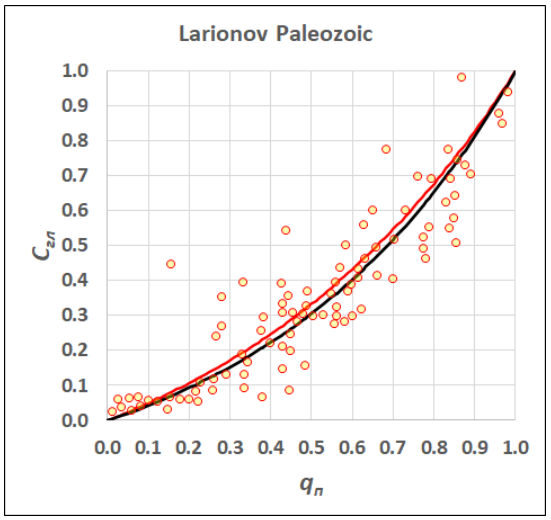

Figure 3. Larionov's graphical function for Paleozoic rocks in the European Soviet Union, west of the Ural mountain range. The anonymous creator of the fitting function (equation 6) chose A = 2.0 as the value for the fitting parameter, yielding the red curve. A fitting parameter that minimizes the sum of the squared residuals is A = 2.37, yielding the black curve. As can be seen, there is not much difference. The reason for the choice of 2.0 is unknown.

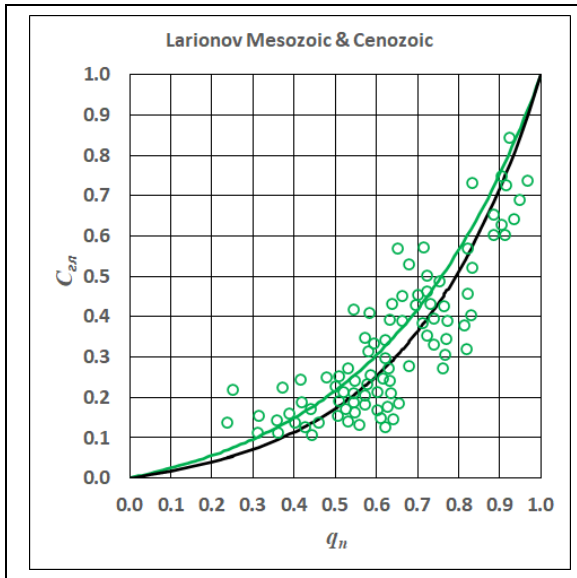

Figure 4. Larionov's graphical function for Mesozoic and Tertiary rocks in the southern Soviet Union, and the underlying data, shown in green. The anonymous creator of the fitting function (equation 6) chose A = 3.7 as the value for the fitting parameter, yielding the green curve. A fitting parameter that minimizes the sum of the squared residuals is A = 4.52, yielding the black curve. The reason for the choice of 3.7 is unknown.

The above observations indicate that a *single* functional form with the variation of a single parameter is adequate to model the Larionov, Stieber, and Clavier et al. data and curves. The implication is that such a function is also adequate to fit any existing or future data by variation of its single parameter.

A Parametric Fitting Function. Bezier curves provide a means to reproduce the four standard functions even more closely than any choice of the three functions above.

The second order Bezier curve (Havil, 2019) specialized to 0 and 1 as the choices for the interval boundary are

$$I_{GR} = x_1 - (1-t)^2 x_1 + t^2 (1 - x_1) \qquad (9)$$

and

$$V_{sh} = y_1 - (1-t)^2 y_1 + t^2 (1 - y_1) \qquad (10)$$

with x_1 and y_1 chosen to best fit the data or curve. The parameter t varies from 0 to 1. All of the four standard curves are fit within "eyeball" accuracy with the Bezier curves. I found the values in the table B1, Appendix B, to work very well. Figures comparing the Bezier curves to the standard transforms are found in Appendix B.

INVERSE TRANSFORMS

The generalized functions have inverses useful for modeling. These are

$$I_{GR} = \frac{\ln\left[\left(2^A - 1\right)V_{clay} + 1\right]}{A \ln 2} \qquad (11)$$

$$I_{GR} = \frac{B}{1/V_{sh} + (B - 1)} \qquad (12)$$

$$I_{GR} = \sqrt{\left[(C+1)^2 + C^2\right] - \left((C+1) - V_{sh}\right)^2} - C \qquad (13)$$

for Larionov, Stieber, and Clavier et al., respectively. This permits the plotting of gamma ray index against shale or clay volume. This plot is shown for all cases in figure 7. What the cases show is that the rate of increase of radioactivity decreases with increasing shale volume. This non-linearity requires a physical explanation. To my knowledge this has not been attempted, although Katahara (1995) alludes to the need for such a model: "if a strong *G*– V_{sh} nonlinearity is actually a property of the formation, then either shale composition or sand composition, or both, must vary with shale volume."

DUAL SILT MODEL

Geologic Modeling. I begin by hypothesizing the characteristics of the rock responsible for the concave down response curves in figure 7. I divide the source of the radioactivity into three components: a radioactive sand with minimal radioactivity, and a shale containing a radioactive clay with a much higher intrinsic radioactivity. The radioactivity of these two components is assumed to vary linearly with the fractional volume of these

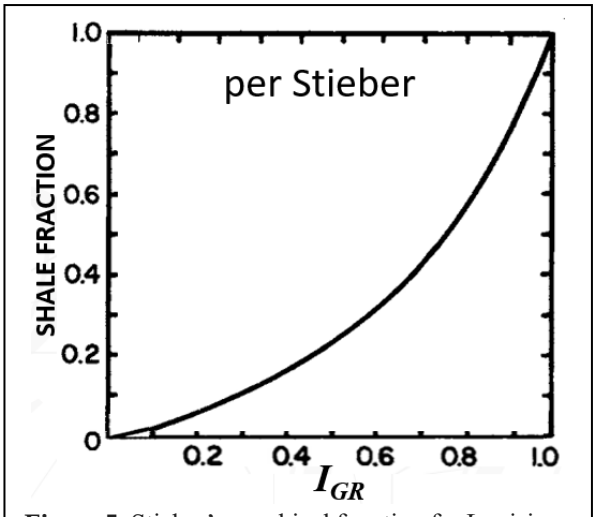

Figure 5. Stieber's graphical function for Louisiana Gulf Coast rocks. (modified from Stieber)

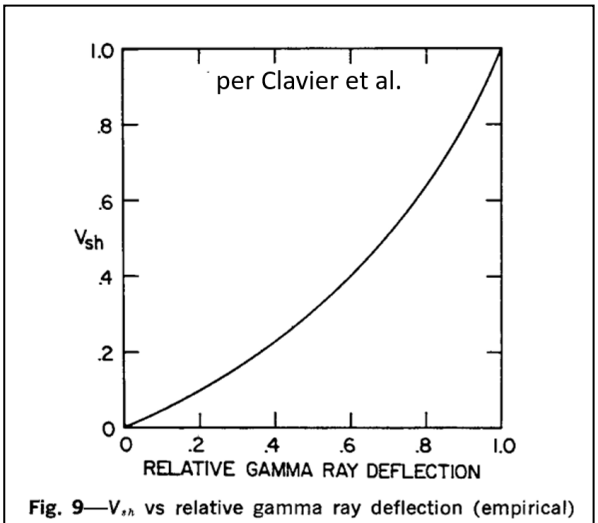

Figure 6. Clavier et al.'s graphical function for Middle East rocks. (modified from Clavier et al.)

components. The sum of the contributions of these two components will also vary linearly with their factional volumes. The third source of radioactivity is the silt component of the shale. I divide the silt into heavy minerals, such as zircon, which is very radioactive, and "ordinary" silt-forming minerals comprising quartz and other weakly radioactive silt-sized grains and crystals. The goal of the discussions below is to provide a plausible verbal description of a physical model, and then to endow the model with mathematical form.

Physical Model. My objective is to posit a model comprising common minerals of differing intrinsic radioactivity. My choice of minerals is quartz to represent rock-forming minerals, illite to represent clay, and zircon to represent a radioactive trace mineral.

Shale Model. In this model the ratio of silt to clay in shale is fixed, but the fraction of highly radioactive silt to slightly radioactive silt varies. What is a mechanism for this variation?

The variability in "excess" radioactivity (defined in figure 16 and the text on page 9) needs a physical explanation. I propose to use zircon as the silt fraction whose radioactivity varies. Zircon is an erosion-resistant mineral with a density 2 g/cm^3 greater than quartz and a Mohs hardness of 7.5 versus 7.0 for quartz. Uranium and thorium are present as inclusions in the zircon crystal. Other uranium and thorium bearing heavy minerals with hardness less than quartz are less likely to survive transport and are not considered in the model. Significantly for this model, measured in API units, zircon is 43 times more radioactive than the clay illite (3773.15 vs. 87.5 API). These facts are recorded in Table 1.

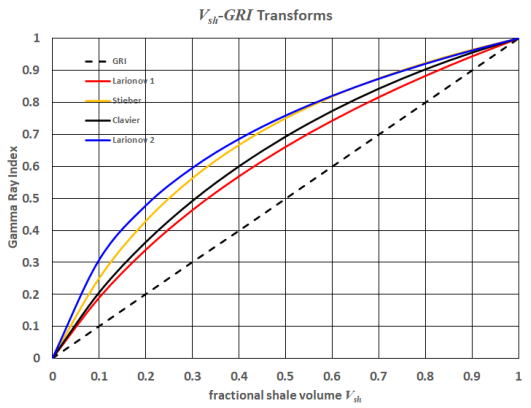

Figure 7. Relationship indicating that the intensity of gamma radioactivity diminishes with shale volume.

The need is for a mechanism to account for high levels of radioactivity associated with dilute amounts of silt, diminishing to lower radioactivity with more concentrated volumes of silt. The geological situation for deposition involves water flowing at rates varying in time, carrying sediment loads that also vary with time, and the erosion and – particularly – the settling, of those sediments. The variation in time scale for individual (and packages of) layers is enormous, from laminations that could be due to transient events lasting minutes to hours, to accumulations of laminations deposited over decades or millennia. Any model will be necessarily highly over-simplified.

How will these loose, detrital components be put together in a rock? In particular, let us consider the kind of laminated sand-shale sequences that can host accumulations of petroleum liquids and gasses. For the source of the sediment loads in streams and rivers, we look to highlands where igneous, metamorphic, and sedimentary rocks are exposed to erosion. A combination of mechanical and chemical weathering produces the finer-grained minerals (e.g., zircon, quartz, illite), capable of bulk transport in water, that will be deposited downstream.

Consider a stream bottom with ripples as shown in figure 8. The scale of the ripples is a few centimeters in height, and ten or so centimeters crest-to-crest. The diagram is highly schematic, but serves to illustrate that downstream of each ripple crest is a trough where dense minerals can accumulate. The surface flow in the troughs will tend to be turbulent, but low-energy compared to water higher in the stream. These low-energy eddies are insufficient to mobilize the heavy mineral fraction that settles into the trough, and so these minerals tend to remain in the trough. Figure 9 is a photograph illustrating the collection of material in troughs between ripples.

	GR(API)	density	hardness
quartz	0	2.65	7
illite	87.5	2.75	1.5
zircon	3,773.15	4.7	7.5

Table 1. Some properties of the minerals in the model described in this article. On the absolute hardness scale Mohs 7.5 is 150 percent harder than Mohs 7.0.

(http://webmineral.com/data/Zircon.shtml#.X11ffbHPxPY)

The ripples will generally be transient in the sense that they will migrate. Depending upon stream speed they can migrate down- or upstream. Figure 8 considers downstream migration. What, then, happens to the placers as the ripples migrate?

Figure 10 illustrates the creation of a zircon rich lamination as a ripple set migrates downstream. The upper panel in the figure outlines where heavy minerals, including zircon, would tend to accumulate in the trough at the base of an upstream crest. However, as the ripples migrate downstream, the dense material will be more or less immobile at the water speed that gives rise to the ripples. This means that the migrating ripple will tend to bury the placer as the ripple migrates. Thus, a lamination is created as the ripples migrate downstream.

Hjulström's Curve. The deposition of placer materials depends upon the size and density of the material, the depth of the stream, and the speed of the flow. These parameters are modeled by the Hjulström diagram (figure 11). For quantitative use in fluvial dynamics Hjulström's (1935) curves are obsolete, but as a heuristic device they meet the needs of this discussion.

The Hjulström curves are graphed upon a bi-logarithmic plot with particle size on the horizontal axis and stream speed on the vertical axis. Since there is no reference in the usual plot to account for the particle density, the plot is for a single particle density. Therefore, materials of differing density will require different plots. Likewise, the plot is for a single stream depth. However, for qualitative use of the plot, the stream depth will not matter for constant depth. The shape of the curves will be roughly the same.

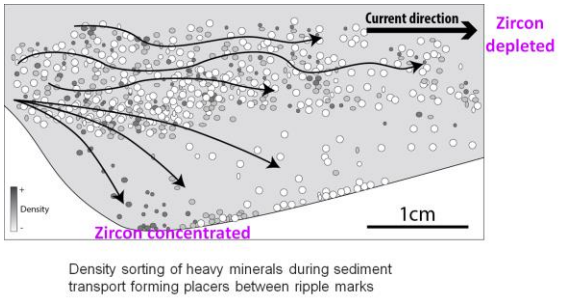

Figure 8. Mechanism for concentration of dense minerals in ripple troughs in a stream flowing to the right. Both the bed load and the suspended load continuing to the right are depleted in the dense mineral, represented here by zircon. (see endnotes for attribution)

The two curves form an envelope between which particles of a given size are mobile in the stream. The lower curve gives the speed at which particles of a given size settle out of the bed load of the stream; the upper curve gives the stream speed it takes to remobilize the same particle from the sediment. So, according to the diagram, once a particle has settled at a certain steam speed, it will not be remobilized until the stream speed is considerably faster than the settling speed.

We are concerned with particles of similar size but significantly dissimilar densities; namely, quartz and illite on the one hand, versus zircon on the other. I take the most frequently reproduced Hjulström diagram (as found on the internet) to be applicable to quartz and illite. To customize the plot for the greater density of zircon, I shift the curves in the diagram up. This means the settling speed for zircon is increased over that of illite and quartz.

To model the zircon curves I have chosen a particle size of 2 mm, and shifted the zircon curve up to where the settling speed for zircon is equal to the mobilization speed for quartz (figure 12). This moves the curve qualitatively in the correct direction, but the amount of the shift is just a guess. The amount of the shift does not affect the qualitative sense of the argument to be made below.

Consider a stream flowing at 55 cm/sec or greater. In this case, there is no deposition from the sediment load. However, if the stream occasionally slows to below 55 cm/sec, zircon will precipitate from the suspended and

Figure 9. Accumulations of placer material deposited in ripple troughs following a rainstorm near Houston, Texas.

bed loads. The stream would have to slow considerably more before quartz and illite silt were not supported by the fluid, so accumulation of zircon-rich sediment is favored under such conditions. Further, the remaining bed and suspended loads transported downstream are depleted in zircon concentration, so downstream sediments will be depleted in zircon. Also, speaking in generalities, the elevation gradient will diminish downstream, leading to a slowing of the stream and consequently higher probability that conditions favorable to deposition of placers of lighter minerals and laminations will occur, thus increasing the number of laminations per unit of depth.

Thus, I argue that upstream there will be fewest laminations with highest individual zircon concentration while farther downstream the occurrence of silt laminations will be more voluminous, but with the laminations depleted in zircon concentration. Finally, still farther downstream silt and clay may tend to dominate the sediment volume, but the silt will be most depleted of zircon and have least radioactivity due to uranium derived from affiliation with zircon. I attempt to capture the essence of this argument in figure 13. The figure caption provides further explanation. Figure 14 and its caption are a visualization and explanation of the distribution of layers for the proposed concentrations of zircon. Figure 15 gives the fractional volume representation of sand, silt, and clay for this model.

The radioactivity due to quartz and illite will be strictly proportional to the amount of quartz and illite present in the sediment and therefore a linear function of clay volume. The radioactivity of the silt component will vary with the concentration of zircon.

The final objective is to quantify the partitioning of the silt into its two (more radioactive vs. less radioactive) components to account for the shape of the curves in figure 7.

This proposed mechanism to explain observations of excess radioactivity where they occur is admittedly crude, and a first attempt. I solicit criticisms and fondly imagine that arguments and efforts to disprove, improve, or replace this model will follow the publication of these ideas.

Mathematical Model. The mathematical model is a description of figure 16. The Stieber curve from figure 7 is chosen to illustrate the model. The object will be to find a variable radioactivity for the silt fraction of the rock that can account for observed gamma ray non-linearity. The first step is to replot the Stieber curve in terms of

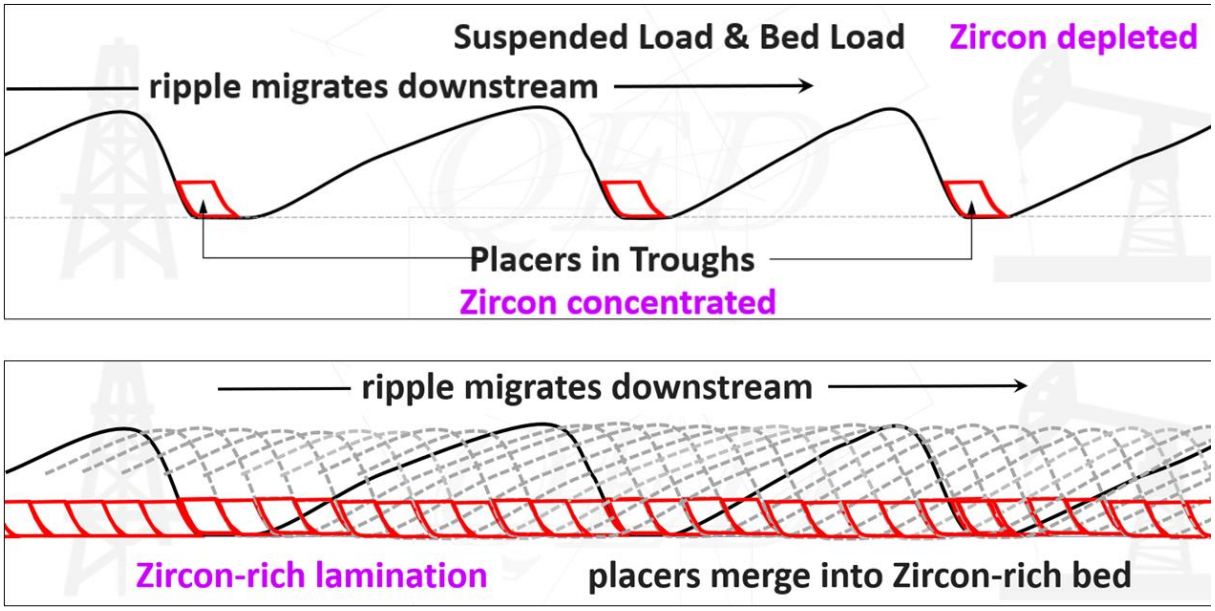

Figure 10. In the upper panel a ripple set is illustrated. Flow is to the right. Heavy material (e.g., gold; zircon, shown by red outline) tends to collect in the troughs between the ripple crests, and is removed from the bed load, which continues to the right depleted in the heavy material. The lower panel illustrates how the heavy material can accumulate into a lamination as the ripples migrate downstream. Under appropriate conditions the zircon-rich layer can be preserved. Sediments deposited further downstream will be less zircon-rich.

gamma ray intensity rather than gamma ray index. Let the gamma ray intensity be denoted by γ. The gamma ray index is expressed in terms of γ as

$$I_{GR} = \frac{\gamma_{log} - \gamma_{min}}{\gamma_{max} - \gamma_{min}} . \qquad (14)$$

The gamma ray curve as recorded on the log in terms of I_{GR}, maximum and minimum gamma ray values is

$$\gamma_{log} = (\gamma_{max} - \gamma_{min}) I_{GR} + \gamma_{min} . \qquad (15)$$

Thus, we can rescale the curves in figure 7 by selecting values for γ_{min} and γ_{max}. In this case I have chosen as typical values, γ_{min} = 15 and γ_{max} = 120 API units. Physically, the gamma ray intensity recorded on the log is the volume-weighted average of the gamma ray intensity of each component weighted by its volume fraction, or

$$\gamma_{log} = \gamma_{sand} V_{sand} + \gamma_{silt} V_{silt} + \gamma_{clay} V_{clay} . \qquad (16)$$

The quartz fractional volume and radioactivity are a maximum at V_{sh} = 0 and diminish linearly to zero at V_{sh} = 1. The clay fractional volume and radioactivity is a minimum at V_{sh} = 0 and increases linearly to V_{sh} = 1. In this model the clay fractional volume is 60% of the shale fractional volume, the remaining 40% of the shale fraction is allotted to silt. The silt volume fraction is the sum of zircon and quartz fractional sub-volumes $V_{silt} = v_{zir\_silt} + v_{qtz\_silt}$. Note that quartz and clay radioactivity are linearly decreasing, and increasing, functions of V_{sh}, respectively. The silt volume comprises a strongly radioactive component v_{zir_silt} and a weakly radioactive component v_{qtz_silt}, thus

$$\gamma_{silt} = \gamma_{zir\_silt} v_{zir\_silt} + \gamma_{qtz\_silt} (V_{silt} - v_{zir\_silt}) . (17)$$

(The practical matter of assessing the parameters on the right of this equation is not addressed in this paper. It is not immediately obvious how, or even whether, this could be done. However, I proceed to show how a theoretical model can be constructed.) I attribute all of the non-linear variability of the radioactivity to the zircon silt component. Since this component of radioactivity is added to the otherwise linear responses of sand and clay, I call it the "excess" radioactivity. For simplicity in this first example model, I have taken γ_{qtz_silt} to be zero and assign the entire source of radioactivity to the zircon silt component. Thus

$$\gamma_{qtz\_silt} \equiv 0 , \qquad (18)$$

and

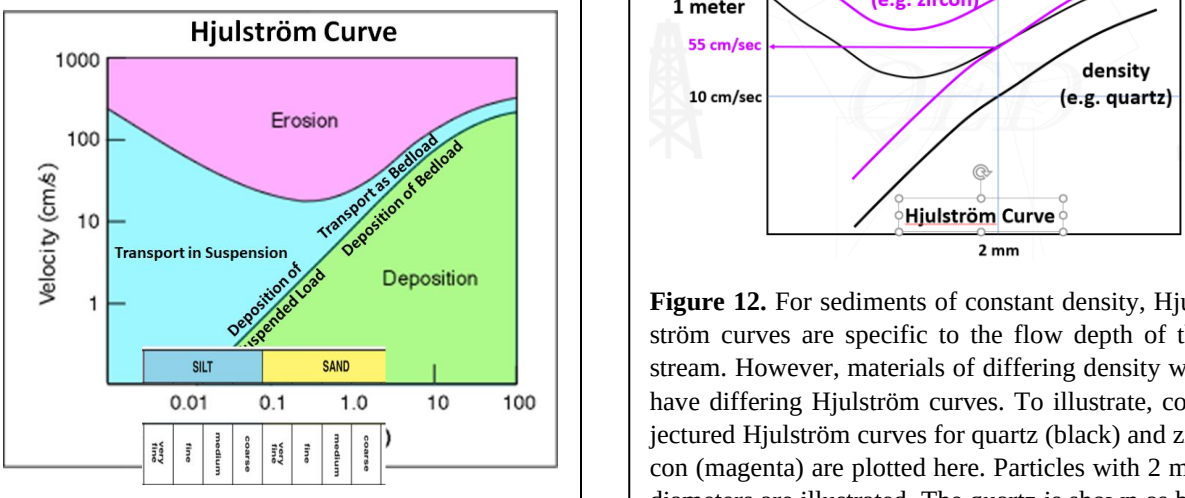

Figure 11. The Hjulström curve models the removal, transport and deposition of material in a sedimentary environment. The chart is for a specific depth of flowing water and material of a specific density. The boundaries between regions for fixed water depth shift up as particle density increases. The illegible labels under silt and sand are, right-to-left: coarse; medium; fine; very fine. These are repeated for silt.

Figure 12. For sediments of constant density, Hjulström curves are specific to the flow depth of the stream. However, materials of differing density will have differing Hjulström curves. To illustrate, conjectured Hjulström curves for quartz (black) and zircon (magenta) are plotted here. Particles with 2 mm diameters are illustrated. The quartz is shown as being in the bed and suspended loads above a flow rate of 10 cm/sec, whereas the zircon is deposited at 55 cm/sec becoming part of the sediments while the quartz is still being transported down to 10 cm/sec. I have no data to support this figure, but it is based upon reasonable conjecture and extrapolation from available literature.

$$\gamma_{silt} \equiv \gamma_{zir\_silt} v_{zir\_silt} . \quad (19)$$

The excess gamma ray component is a function of shale volume

$$\gamma_{excess} \equiv \gamma_{excess}\left(V_{sh}\right). \quad (20)$$

Based upon these considerations the gamma ray intensity of the zircon component can be modeled as the product of the fractional volume of silt and the intrinsic radioactivity of the zircon silt fraction, or $\gamma_{excess}(V_{sh})$ = $V_{silt}(V_{sh})\,\gamma_{zir\_silt}$. γ_{zir_silt} varies with V_{sh} since both γ_{excess} and V_{silt} vary with shale volume fraction. Thus

$$\gamma_{zir\_silt} = \frac{\gamma_{excess}\left(V_{sh}\right)}{V_{silt}\left(V_{sh}\right)} . \quad (21)$$

The gamma ray intensity of the silt is plotted in figure 17. Equation (21) blows up at $V_{sh} = V_{silt} = 0$; however, a polynomial of third or fourth order can be fit to the nine data points computed using equation (21). This polynomial can then extrapolated to estimate the silt radioactivity at $V_{sh} = 0$. The fraction of silt that is zircon is estimated as the ratio of gamma ray intensity to the

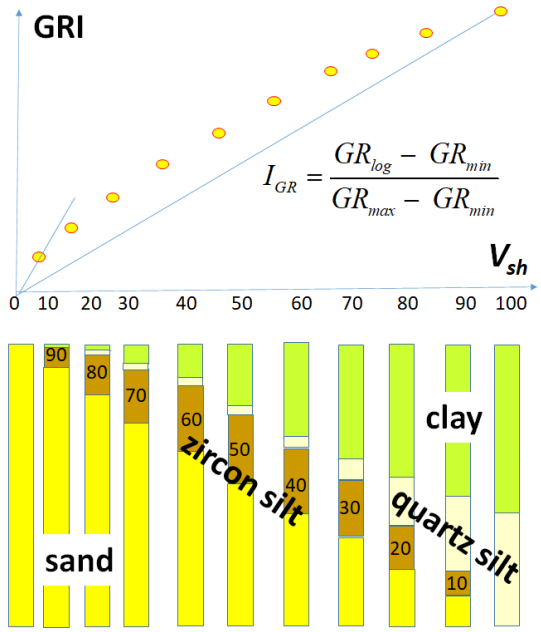

Figure 13. The observed excess radioactivity varies from a minimum (approximately zero) at minimum shale volume to a maximum for intermediate fractional shale volumes, and back to a minimum at maximum shale volume. This is shown at 11 points by the graph at the top of the figure. The fractional volumes of sand, silt, and clay vary linearly, but the silt is compounded from two components. The zircon component begins as a large fraction of a small percentage of the silt at the maximum fractional sand volume, and is linearly reduced to a small fraction of the maximum percentage silt as a fraction of rock volume. This is shown as the brown fraction of the silt. As a fractional volume of the whole rock, the zircon component begins as a small fraction, grows to a maximum, and diminishes back to a small fraction.

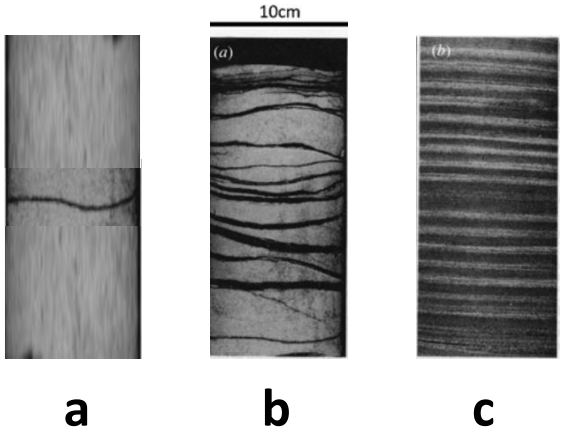

Figure 14. Plausibility arguments for zircon distribution. For **a**, the stream speed is highest and zircon concentration in the bed and suspended loads is also high. When stream speed occasionally slows to values too low to transport larger zircon crystals they settle into isolated laminations. The zircon concentration is high in the lamination, but there are few laminations. Fractional mass of zircon in the bulk sediment is low. The sediments in **b** are downstream from **a** where stream speed is slower and more variable allowing for the more frequent deposition of fine-grained zircon-depleted silt and clay. Although the zircon concentration per lamination is less than upstream deposits, there are many more laminations and the fractional mass of zircon is high, reaching a maximum at some value of fractional silt volume. For **c**, the stream speed is lowest and the zircon mass fraction is least, approaching zero. The resulting laminations are most abundant in fractional volume, but also most zircon depleted.

maximum gamma ray intensity due to the zircon; i.e., $v_{zir\_max}\big|_{V_{sh}=0}$. Thus

$$v_{zir\_silt} = \frac{\gamma_{zir\_silt}\left(V_{sh}\right)}{\gamma_{zir\_max}}. \qquad (22)$$

Finally, the fractional volume of the zircon silt is given by $V_{zir} = V_{silt} \cdot v_{zir\_silt}$. and plotted in figure 18.

I use Stieber's function (arbitrarily selected from among the four candidates for convenience; any of them could have been used in this interpretation) to illustrate the model. Radioactivity which is over and above the linear component contributed by sand and clay is called the "excess" radioactivity. The excess varies from zero in a sandstone to a maximum at intermediate shale volumes, and reduces back to zero as the shale fraction increases to 100 percent. This is consistent with the geological model posited earlier in the paper.

Figure 15 is replotted as figure 18 showing the silt fractional volume partitioned into the quartz and zircon fractions required to produce the observed non-linear gamma ray response.

The mathematical model is captured in the above nine equations. I make no claims for the model other than it does the job of fitting the data, and gives concrete form to the arm-waving geological explanation presented in the Physical Model and Shale Model sections. It is admittedly an ad hoc procedure.

In Appendix E I provide an algorithm for reproducing figures such as figure 18.

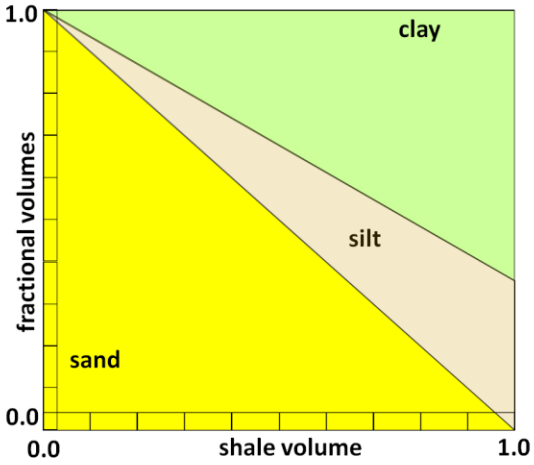

Figure 15. The linear composition model of a sand-shale mixture. The shale fraction is a mixture of silt and clay.

The physical model needs a rationale such as is to be found in figure 19, accounting for the diminishing concentration of radioactive material as it moves from its sources in highlands to its final deposition in rivers, estuaries, swamps, deltas, etc.

CONCLUDING REMARKS

Our industry's ubiquitous mistranslation of Larionov's sample ages should be corrected in future citations of his work. The error is not merely in the mistranslation of a word, but also in moving the boundary from Mesozoic-Cenozoic back 147 million years to the Paleozoic-Mesozoic. Since these 147 million years contain the deposition of about 50 percent of the source rocks on the planet (Soua and Chihi, 2014), if a distinction is to be made in the use of Larionov's transforms, this one seems significant.

No right-minded scientist could accept as proven a hypothesis based upon such skimpy data as the non-linearity of the gamma ray index – shale volume transforms published in the literature. We should keep in mind that

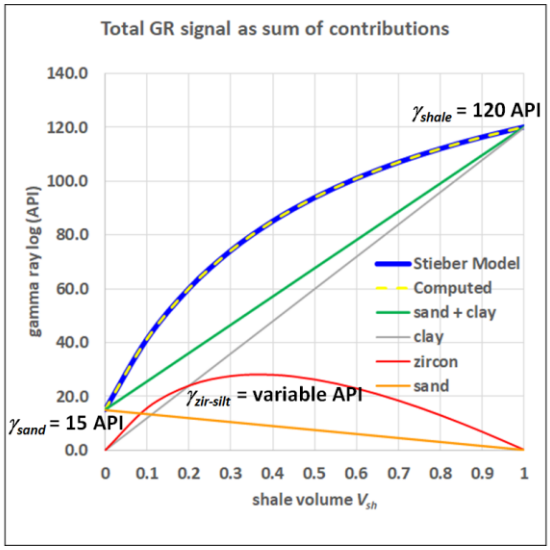

Figure 16. The Stieber model (blue curve) is used to illustrate the dual silt model. The gamma ray index is decomposed into a minimum, a maximum, and intermediate (or log) values. The minimum and maximum are chosen to be typical gamma ray values for clay-free sand and shale. The Stieber curve is modeled as the sum of radioactivity due to a sand component (yellow line), a clay component (gray line), and "excess" radioactivity due to a variable component attributed in the model to zircon concentration (red curve). The sum of sand and clay γ intensities is shown by the green line.

two of the standard transforms were first invoked in the service of pulsed neutron decay time log interpretations around 1970, and that there have been no other such claims in the literature in the intervening 50 years. However that may be, petrophysicists are sometimes obliged to consider the hypothesized relationship in their efforts to reconcile incomplete, inaccurate, and inconsistent data. Clearly the standard formulas are physically meaningless, representing attempts by three isolated individuals to fit functions to their individual data sets. All used graphical functions, which honor the boundary conditions and describe the trends or functions they observed. Had they been aware of one another, they might have agreed upon a single transform. The four trends comprising the standard formulas do seem capable of being reduced to a single function and this should be done strictly for the sake of parsimony. Empirical formation evaluation is rife with arcane formulas unsupported by physics and we should reduce the number where we can. Although each collection of data may require a different variation of a curve, this variation is achievable by varying a parameter (or two) in a standard functional form without the use of different functions.

Finally, I have hypothesized a physical model (Figure 18) invoking physical and geological principles (Figure 19). My use (or misuse) of these principles, and omission of others, can and should be, challenged. Since there are essentially only four graphical functions to use for comparison to the model, falsifying it may possibly be done from the comfort of arm chairs by refuting its assumptions, but if not this then it requires the collection and analysis of new data. Since there has not been interest in investing in this analysis during the past 50 years, it probably will not be undertaken in the next 50 either. However, what I hope will happen is to kindle an interest in a theoretical analysis of my proposed mechanism, to refute it or extend it or refine it, or replace it with a more viable mechanism.

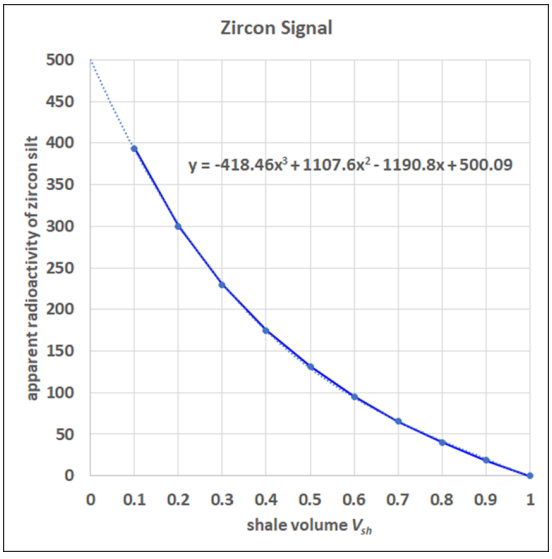

Figure 17. The apparent radioactivity of the zircon fraction is a maximum at minimum shale volume and a minimum at maximum shale volume. The values in this diagram are estimated from the model.

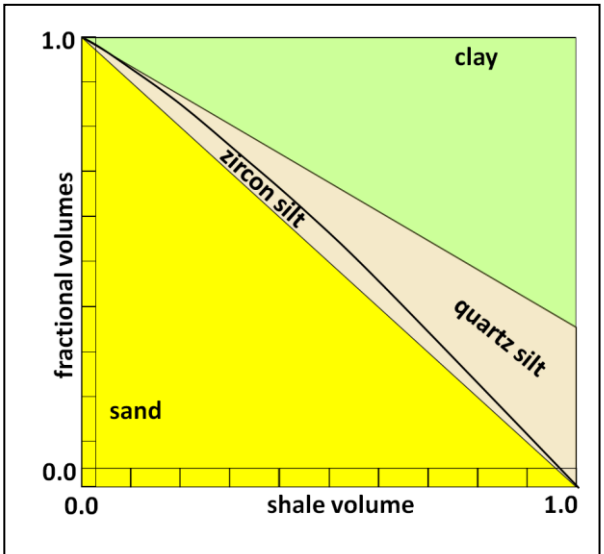

Figure 18. The dual-silt model postulates a silt fraction comprising the ubiquitous rock-forming minerals (e.g., quartz) and less abundant radioactive heavy minerals, in this case represented by zircon.

ACKNOWLEDGEMENTS

My sincere appreciation to colleagues Quinn Passey for illuminating discussions regarding shales and zircon and Elton Frost for sharing his encyclopedic knowledge regarding early publications on the relationship between gamma ray intensity and shale volume.

REFERENCES

Bush, Robert E., and Mardock, E. S., 1950, The Quantitative Application of Radioactivity Logs, *Petroleum Transactions*, AIME, Vol. 192, pp. 191-198.

Bhuyan and Passey, 1994, Clay Estimation from GR and Neutron-Density Porosity Logs, *Transactions* of the SPWLA 35th Annual Logging Symposium, paper DDD.

Clavier, C., Hoyle, W., Meunier, D., 1971, Quantitative Interpretation of Thermal Neutron Decay Time Logs: Part I. Fundamentals and Techniques, *Journal of Petroleum Technology*, Vol. 23, No. 6, pp. 743-755.

Havil, Julian, 2019, *Curves for the Mathematically Curious*: *An Anthology of the Unpredictable, Historical, Beautiful, and Romantic*, Princeton University Press.

Heslop, A., 1974, Gamma-ray Log Response of Shaly Sandstones, *The Log Analyst*, Vol. 15, No. 5, pp. 16-21.

Hjulström Filip, 1935, *Studies of the morphological activity of rivers as illustrated by the River Fyris*, doctoral thesis.

https://en.wikipedia.org/wiki/Bézier_curve

https://en.wikipedia.org/wiki/Hjulström_curve

Katahara, K. W., 1995, Gamma Ray Log Response in Shaly Sand, *The Log Analyst*, Vol. 36, No. 4, pp. 50-55.

Ларионов, В. В., 1969, Радиометрия Скважин [Borehole Radiometry], НЕДРА, Москва [NERDA, Moscow].

Poupon, A., Gaymard, R., 1970, The Evaluation of Clay Content from Logs, *The Log Analyst*, Vol. 11, No. 6, November-December, pp. 18-25.

Soua, M., Chihi, H., 2014, Optimizing exploration procedure using Oceanic Anoxic Events as new tools for hydrocarbon strategy in Tunisia, in: *Advances in Data, Methods, Models and Their Applications in Oil/Gas Exploration*, Chapter 2 (pp.25-89), eds. Said Gaci, Olga Hachay, Science Publishing Group

Stieber, S. J., 1970, Pulsed Neutron Capture Log Evaluation: Louisiana Gulf Coast, American Institute of Mining, Metallurgical and Petroleum Engineers, SPE 2961

www.spwla.org, video gallery, The skeptical petrophysicist webinar, hour-long video: Gamma Ray – Shale Volume Transforms.

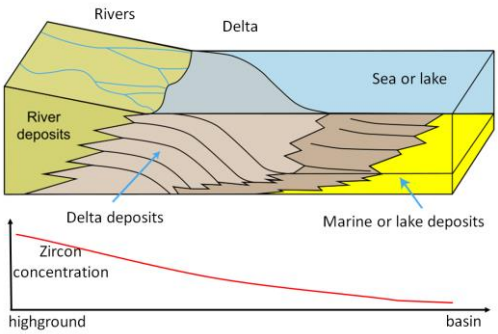

Figure 19. The concentration of radioactive zircon in a sedimentary system is high at its sources in highlands where it is eroded from igneous and sedimentary rocks, but can be even higher where it is concentrated by density differentiation in placer deposits. The concentration in distal offshore deposits is minimal or nil due to the high density of the mineral. (https://www.jpl.nasa.gov/spaceimages/details.php?id=PIA19071)

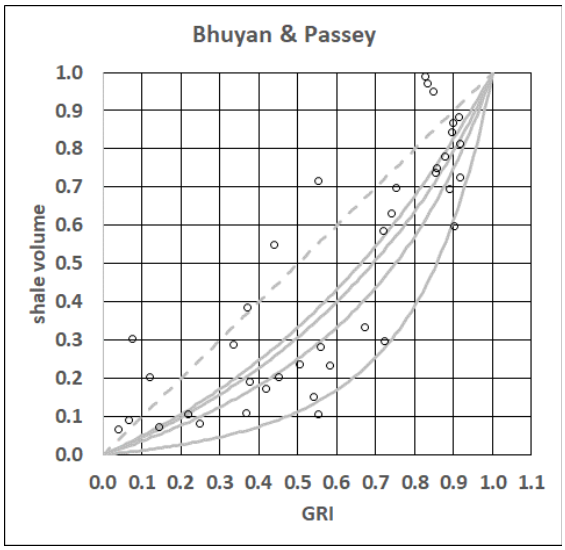

Figure A1. The shale volume versus gamma ray index plot for the data of Bhuyan and Passey (1994). These data are from the Frio formation in Louisiana and Texas, and Cretaceous rocks in Utah. The gray lines are the standard transforms. Since the data are not identified as to provenance, it is not possible to make specific observations. However, it is clear that the data volume encompasses both linear and nonlinear regions of the chart.

APPENDIX A

Other than the Larionov data, the only published data that I am aware of is that of Bhuyan and Passey (1994; see figure A1).

Their data is sparse and represents more than a single formation ("Frio formation Texas and Louisiana" and "Cretaceous rocks in Utah") and thus exhibits considerable variation. However, one can see that this data set could support both linear and non-linear relationships between gamma ray index and shale volume, depending upon which rocks represent which formations.

APPENDIX B

Bezier curves provide a means to smoothly interpolate data, while dispensing with the need to invent ad hoc functions to fit roughly quadratic curves to scatter-prone data sets. The Bezier curves are no less ad hoc than any of the "standard" curves used in GRI-V_{sh} transforms, but have the advantage that only one function is required; changes in the function's parameters are used to produce the fits. Although I have not done so here, the parameters can be chosen to minimize the sum of squared residuals to conform to the method of least squares. Of course there is no physical significance to these functions; they merely fit a quadratic function to data sets that follow roughly quadratic trends.

Second order (i.e., quadratic) Bezier functions have three fitting parameters in general (e.g., x_0, x_1, x_2). These are chosen to give the desired shape to the curve. In our case, x_0 = 0 and x_2 =1 in order to fit the boundary condition that the function equal 0 when I_{GR}, V_{sh}, and the parameter t = 0, and equal 1 when I_{GR}, V_{sh}, and the parameter t = 1. With these substitutions made, the form of the function is, for gamma ray index

$$I_{GR} = x_1 - (1-t)^2 x_1 + t^2 (1 - x_1), \qquad \text{(B.1)}$$

and for shale (or clay) volume

$$V_{sh} = y_1 - (1-t)^2 y_1 + t^2 (1 - y_1). \qquad \text{(B.2)}$$

The parameters x_1 and y_1 are varied to fit the data. The values found that work well are listed in table B1.

Inspection of figures B.1 through B.4 will show that for use in oil-field calculations, there are no practical differences between the "standard" curves and the Bezier curves.

	x_1	y_1
Larionov P	0.65	0.32
Clavier	0.69	0.29
Larionov M&C	0.71	0.13
Stieber	0.76	0.23

Table B1. The x_1 and y_1 parameters for fitting the standard transforms using Bezier curves.

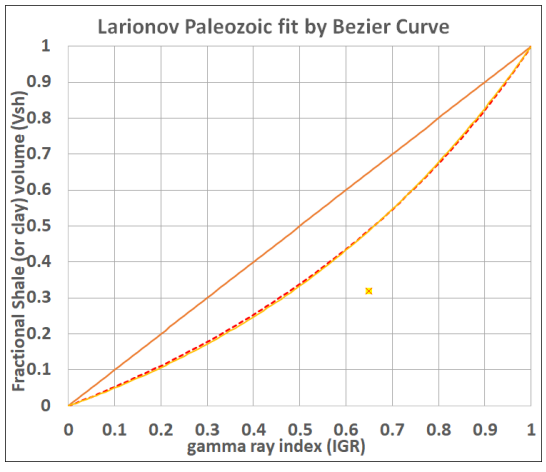

Figure B1. Bezier curve fitting of "standard" Larionov Paleozoic curve.

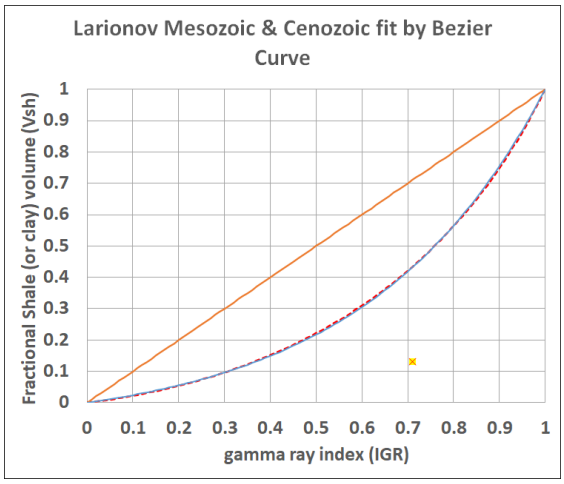

Figure B2. Bezier curve fitting of "standard" Larionov Mesozoic and Cenozoic (i.e., "Tertiary") curve.

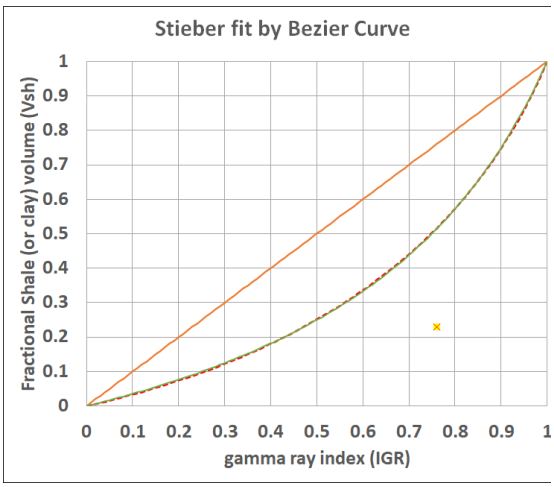

Figure B3. Bezier curve fitting of Stieber's curve.

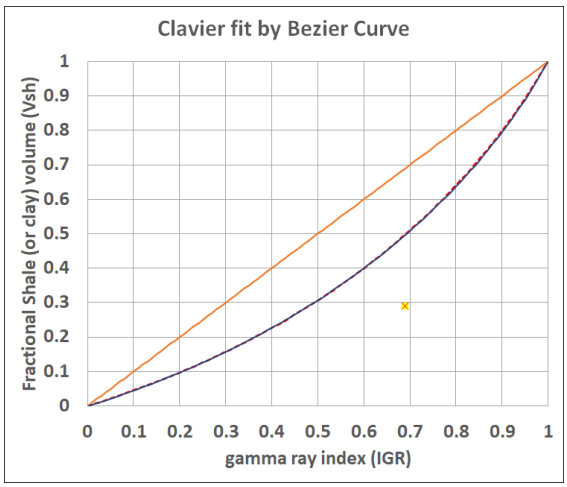

Figure B4. Bezier curve fitting of Clavier's curve.

APPENDIX C

A listing of the data points in Larionov's Figure 23.a .

Larionov Paleozoic

#	V_{sh}	q_n (I_{GR})	#	V_{sh}	q_n (I_{GR})	#	V_{sh}	q_n (I_{GR})
1	0.04196	-0.01641	33	0.21998	0.39998	65	0.3178	0.62183
2	0.02556	0.01354	34	0.39118	0.4262	66	0.55979	0.62785
3	0.05863	0.02762	35	0.30807	0.42858	67	0.46054	0.63274
4	0.03562	0.03435	36	0.33348	0.429	68	0.59874	0.65084
5	0.06413	0.05384	37	0.20935	0.42929	69	0.49434	0.65995
6	0.0284	0.05946	38	0.14758	0.43033	70	0.41295	0.66172
7	0.0667	0.07589	39	0.54318	0.43943	71	0.77291	0.6842
8	0.04079	0.08205	40	0.35557	0.44256	72	0.40415	0.69937
9	0.05775	0.10102	41	0.08425	0.4457	73	0.51506	0.70395
10	0.05397	0.12372	42	0.19804	0.45025	74	0.6008	0.72959
11	0.03057	0.14716	43	0.2477	0.45049	75	0.69527	0.76054
12	0.06472	0.15467	44	0.30664	0.45544	76	0.49104	0.77393
13	0.44522	0.15612	45	0.28078	0.46517	77	0.52222	0.7743
14	0.05807	0.17858	46	0.30345	0.47873	78	0.46226	0.7813
15	0.05947	0.20005	47	0.15687	0.48456	79	0.55241	0.789
16	0.08044	0.21601	48	0.32724	0.48871	80	0.69163	0.79517
17	0.05164	0.22218	49	0.36824	0.48961	81	0.62391	0.83026
18	0.10772	0.22894	50	0.29854	0.50383	82	0.77352	0.83694
19	0.08614	0.25953	51	0.30057	0.52947	83	0.5501	0.83854
20	0.11733	0.26109	52	0.36257	0.54872	84	0.69044	0.84231
21	0.24097	0.26796	53	0.27433	0.55711	85	0.57679	0.85029
22	0.3537	0.28028	54	0.39329	0.55924	86	0.64322	0.85279
23	0.2671	0.2809	55	0.2969	0.56112	87	0.50698	0.85437
24	0.13096	0.29143	56	0.3223	0.56153	88	0.74431	0.85684
25	0.18799	0.3298	57	0.43672	0.56967	89	0.97945	0.87008
26	0.39472	0.3325	58	0.28211	0.58092	90	0.72836	0.87605
27	0.1309	0.33558	59	0.49925	0.58473	91	0.70254	0.88996
28	0.09107	0.33706	60	0.36997	0.58983	92	0.87656	0.96031
29	0.16448	0.34369	61	0.38856	0.59925	93	0.84838	0.96946
30	0.25609	0.37764	62	0.29679	0.60169	94	0.93684	0.98076
31	0.06502	0.3808	63	0.43319	0.61384	95	0.98523	1.02099
32	0.29485	0.38393	64	0.40838	0.61581			

Larionov Meso- & Cenozoic

#	shale vol	M & C	#	shale vol	M & C	#	shale vol	M & C
1	0.13611	0.23811	32	0.2041	0.5735	63	0.46257	0.72329
2	0.21691	0.25274	33	0.18106	0.57374	64	0.49944	0.72408
3	0.11155	0.31346	34	0.2318	0.57797	65	0.35313	0.72446
4	0.15303	0.31421	35	0.31362	0.58066	66	0.43155	0.73196
5	0.14083	0.35963	36	0.40812	0.58323	67	0.39478	0.7407
6	0.10974	0.36116	37	0.25494	0.58725	68	0.33027	0.74139
7	0.22391	0.37305	38	0.33336	0.59476	69	0.48708	0.75401
8	0.15841	0.38924	39	0.16639	0.60251	70	0.26944	0.7635
9	0.13668	0.40378	40	0.21132	0.60322	71	0.42383	0.76542
10	0.24279	0.41575	41	0.14804	0.61105	72	0.3052	0.76788
11	0.18522	0.41875	42	0.24603	0.61715	73	0.34325	0.77105
12	0.12542	0.42893	43	0.12396	0.62203	74	0.38936	0.77413
13	0.17049	0.44275	44	0.34055	0.62209	75	0.37712	0.81598
14	0.10599	0.44463	45	0.29563	0.62257	76	0.31958	0.82136
15	0.13495	0.45982	46	0.17471	0.62745	77	0.45669	0.82347
16	0.24693	0.48126	47	0.27036	0.63	78	0.56846	0.82465
17	0.22526	0.50295	48	0.39021	0.63348	79	0.40264	0.83239
18	0.15159	0.50851	49	0.24044	0.63389	80	0.51901	0.83353
19	0.25068	0.50983	50	0.20935	0.63542	81	0.72984	0.83365
20	0.18849	0.51168	51	0.42945	0.64021	82	0.6025	0.88507
21	0.21048	0.52218	52	0.14377	0.64327	83	0.65089	0.88575
22	0.16905	0.5262	53	0.56667	0.65185	84	0.74787	0.90616
23	0.26934	0.53227	54	0.18423	0.65714	85	0.62691	0.90627
24	0.13802	0.53368	55	0.44928	0.66383	86	0.60279	0.91368
25	0.41694	0.54499	56	0.38707	0.6645	87	0.72609	0.91593
26	0.18654	0.54627	57	0.52778	0.67968	88	0.84254	0.92541
27	0.20959	0.54722	58	0.27548	0.68	89	0.64104	0.93591
28	0.16121	0.54773	59	0.42888	0.69623	90	0.68728	0.95091
29	0.24072	0.54927	60	0.45198	0.70195	91	0.73471	0.96947
30	0.13023	0.55999	61	0.38182	0.71343	92	0.80102	1.03193
31	0.34696	0.57316	62	0.56965	0.71737			

Other than the Larionov data, the only published data that I am aware of is that of Bhuyan and Passey (1994; see figure A1) , listed below.

GRI	Wt%Clay	GRI	Wt%Clay
0.04029	3.99	0.58268	14.03
0.066	5.354	0.67272	20
0.07529	18.249	0.7196	35.096
0.12052	12.138	0.724	17.842
0.14397	4.353	0.74043	37.914
0.21809	6.261	0.75339	41.87
0.24964	4.821	0.82602	59.37
0.33495	17.234	0.83289	58.23
0.36719	6.543	0.84668	56.99
0.37067	23.073	0.85319	44.207
0.37722	11.433	0.85815	45.041
0.41767	10.414	0.87795	46.818
0.4401	32.983	0.89063	41.73
0.4513	12.198	0.89684	50.673
0.50567	14.096	0.89984	52.026
0.54204	9.124	0.90131	35.914
0.55183	6.426	0.91271	53.072
0.55199	42.914	0.91636	43.51
0.55908	16.929	0.91751	48.812

APPENDIX D

The captions from Larionov's figures 23 and 43, Chapter 4 of *Borehole Radiometry*. My translations are listed below each caption. The words Paleozoic, Mesozoic, and Tertiary (in Cyrillic font and Russian) are boxed in red. These words are in bold type in the translations. As you see, the data is divided at the Paleozoic-Mesozoic boundary. Tertiary is lumped together with Mesozoic in Figure 43, and not mentioned at all in the figure with the actual data, Figure 23.

Рис. 23. Связь естественной радиоактивности $q_п$ терригенных отложений с глинистостью $C_{гл}$ (*а*) и карбонатных отложений с содержанием нерастворимого остатка $C_{но}$ (*б*).

1 — палеозойские отложения Предуралья и центральных районов СССР; *2* — мезозойские отложения южных районов СССР; *3* — отложения Cr_2 Восточного Предкавказья; *4* — отложения $Cr_2^{sm} + Cr_1^{alb}$ Восточного Предкавказья.

Fig. 23. Relationship (of) natural radioactivity q_n (to) terrigenous sediment with clay $C_{гл}$.
1 – **Paleozoic** sediments from Pre-Urals and central areas of the USSR. 2 – **Mesozoic** sediments from the southern USSR.

Рис. 43. Палетки для приближенной оценки глинистости осадочных горных пород.

а — для палеозойских отложений Предуралья и центральных районов Европейской части СССР; *б* — для мезозойских и третичных отложений южных районов СССР. Шифр кривых — поправочный коэффициент *k*.

Fig. 43. Charts for the evaluation of argillaceous sedimentary rocks.
a – For **Paleozoic** sediments from the Pre-Urals and central European regions of the USSR; *b* – For **Mesozoic** and **Tertiary** sediments from the southern region of the USSR.

APPENDIX E

For clarity I include a step-by-step procedure for constructing the model I have displayed in figure 18.

(0) Begin with gamma ray log data and observe the values of the trendlines for the minimum and maximum values in the interval of interest. Identify $\gamma_{min} \equiv \gamma_{sand}$ and $\gamma_{max} \equiv \gamma_{shale}$.

(1) Select a silt fraction for the shale. Bhuyan and Passey recommend approximately 0.4 for this.

(2) You will need $v_{silt}(V_{sh})$ later in the calculation and you can compute it here.

(3) By solving the resistivity index equation for γ_{log} (or $\gamma_{observed}$), compute γ_{sand} (V_{sh}) and γ_{clay} (V_{sh}).

(4) Then compute the linear component of the gamma ray log: $\gamma_{linear}(V_{sh}) = (1 - V_{sh})\gamma_{sand} + V_{sh}\ \gamma_{clay}$. This is assuming all the radioactivity at $V_{sh} = 0$ is due to the sand component and all the radioactivity at $V_{sh} = 1.0$ is due to clay.

(5) Compute $\gamma_{excess} = \gamma_{observed} - \gamma_{linear}$. Excess gamma ray will be zero at both boundaries and a maximum at some value of shale volume between the boundaries.

(6) In this model we assume that $V_{silt}(V_{sh}) = v_{zir\_silt}(V_{sh}) + v_{qtz\_silt}(V_{sh})$ and $\gamma_{silt}(V_{sh}) = v_{zir\_silt}(V_{sh})\ \gamma_{zir\_silt}(V_{sh}) + v_{qtz\_silt}(V_{sh})\ \gamma_{qtz\_silt}(V_{sh})$; however, to make the model simpler, I assign $\gamma_{qtz\_silt}(V_{sh}) = 0$.

(7) Thus $\gamma_{silt}(V_{sh}) = v_{zir\_silt}(V_{sh})\ \gamma_{zir\_silt}(V_{sh})$.

(8) Now compute $\gamma_{zir\_silt}(V_{sh})$ according to $\gamma_{zir\_silt}\left(V_{sh}\right) = \dfrac{\gamma_{excess}\left(V_{sh}\right)}{V_{silt}\left(V_{sh}\right)}$

(9) The quantity needed for a result in this model is the fractional volume of zircon silt. It is computed using $v_{zir\_silt} = \dfrac{\gamma_{zir\_silt}\left(V_{sh}\right)}{\gamma_{zir\_max}}$.

Figure 18 can now be plotted. Plot $V_{sand} = 1 - V_{shale}$. This is the locus of the sand-shale boundary. Plot $1 - V_{clay}$. This is the locus of the silt-clay boundary. The silt fraction is located between these two lines. The boundary between zircon silt and quartz silt is given by the sum $V_{sand} + V_{silt} \cdot v_{zir\_silt}$.